Small post-perovskite patches at the base of lower mantle primordial reservoirs: Insights from 2-D numerical modeling and implications for ULVZs

Yang Li[1], Frédéric Deschamps[1], and Paul J. Tackley[2]

[1]Institute of Earth Sciences, Academia Sinica, Taipei, Taiwan, [2]Institute of Geophysics, Department of Earth Sciences, ETH Zurich, Zurich, Switzerland

Abstract We perform numerical experiments of thermochemical mantle convection in 2-D spherical annulus geometry to investigate the distribution of post-perovskite (pPv) with respect to the location of primordial reservoirs of dense material in the lowermost mantle. High core-mantle boundary temperatures lead to strong anticorrelation between the locations of pPv and large primordial reservoirs, while low values lead to a pPv layer fully covering the outer core. Intermediate values avoid a full pPv layer but allow pPv phase change to occur within the primordial reservoirs. Through interactions between cold downwellings and primordial reservoirs, low viscosity (weak) pPv leads to the formation of long-lived, thin tails of primordial materials extending laterally at the edges of these reservoirs. Small patches of pPv also form within the primordial reservoir but are short-lived. If primordial reservoirs are enriched in iron, these patches may provide an explanation for the ultralow-velocity zones.

1. Introduction

The present-day Earth's mantle appears to be heterogeneous, the strongest heterogeneities being found at its top (<400 km) and at its bottom, from ~2500 km down to core-mantle boundary (CMB). Seismological studies suggest that different scales of heterogeneities coexist, with small scale (10–100 km) heterogeneities inducing substantial scattering visible in coda waves [e.g., *Rost et al.*, 2015]. In the lowermost mantle (>2500 km), the seismic large-scale structure is dominated by two antipodal large low shear velocity provinces (LLSVPs) beneath Africa and the Pacific [e.g., *Ishii and Tromp*, 1999; *Masters et al.*, 2000; *Ni et al.*, 2002; *Wang and Wen*, 2007; *He and Wen*, 2012], where the shear wave velocity decreases by a few percent compared to its horizontally averaged value. The exact nature of LLSVPs is still not well known, but several hints from seismic observations and geodynamics modeling, e.g., sharp edges and the anticorrelations between shear velocity and bulk sound velocity, suggest that LLSVPs are more likely related to thermochemical structures [e.g., *van der Hilst and Kárason*, 1999; *Masters et al.*, 2000; *Ni et al.*, 2002; *Trampert et al.*, 2004] than to purely thermal variations [*Davies et al.*, 2012]. Much smaller heterogeneities have been observed, mainly in the lowermost 100 km of the mantle. These include the low-velocity zones (LVZs) [*Sun et al.*, 2013], which are several hundred kilometers in length and 80-100 km in height with less than 10% velocity drops, and the ultralow-velocity zones (ULVZs), which are usually several tens of kilometers in height, and where seismic velocities drop by 10 to 30% [e.g., *Wen and Helmberger*, 1998; *Helmberger et al.*, 2000; *Rost and Revenaugh*, 2003; *Thorne and Garnero*, 2004]. So far, ULVZs have been detected locally in various places, in particular, within or at the margins of LLSVPs [*McNamara et al.*, 2010]. Several possible origins have been advocated to explain ULVZs, including partial melting due to different processes [e.g., *Williams and Garnero*, 1996], ponds of partially melted subducted slab basalt, which has a lower melting temperature than pyrolite [*Andrault et al.*, 2014], iron-enriched post-perovskite (pPv) [e.g., *Mao et al.*, 2006], and chemically denser material or mixture. For details on ULVZs' distribution and properties, we refer to reviews by *Garnero* [2000], *Thorne and Garnero* [2004], and *Tackley* [2012].

Another seismic structure that is locally observed in the lowermost 200–300 km above core-mantle boundary is the D″ discontinuity. This discontinuity is characterized by an increase in shear wave velocity by a few percent [*Lay and Helmberger*, 1983] and was proposed to result from an exothermic phase change [*Sidorin et al.*, 1999]. In the meantime, mineral physics studies have shown that under the pressure and temperature conditions of the deep mantle, perovskite may transform to post-perovskite [*Murakami et al.*, 2004; *Oganov*

and Ono, 2004; *Tsuchiya et al.*, 2004]. Due to the strongly exothermic nature of this phase transition, it is usually assumed that post-perovskite is not stable within LLSVPs, which are assumed to be hotter than surrounding mantle [e.g., *Nakagawa and Tackley*, 2005]. The presence of pPv, however, also depends on the temperature at the CMB (T_{CMB}). If this temperature is low enough, pPv may be locally stable at the base of LLSVPs. Interestingly, a recent study [*Nomura et al.*, 2014] suggests a CMB temperature of 3570K $\pm$ 200K, significantly lower than previous estimates. This would favor pPv being widespread above the CMB, including within LLSVPs. In contrast, according to previous numerical experiments [*Li et al.*, 2015] similar to those we performed here, for high CMB temperature (around 4200 K) pPv is unstable throughout the CMB. Furthermore, the stability field of pPv is sensitive to the composition, with iron perovskite transforming at shallower depth, and being stable up to larger temperature at CMB pressure [*Mao et al.*, 2006]. This would favor the formation of pPv patches within LLSVPs, if these structures are enriched in iron, as suggested by compositional models [e.g., *Trampert et al.*, 2004; *Mosca et al.*, 2012]. The presence of pPv within the large primordial reservoirs may have some important implications on the dynamics of the lowermost mantle.

In this study, we investigate the relative distribution of the post-perovskite phase and reservoirs of dense, primordial material (modeling the LLSVPs), and its dependence on the properties of the pPv phase change and on the CMB temperature. We focus mainly on the parameters that from previous work [*Li et al.*, 2015] are known to play an important role on the occurrence and structure of pPv: CMB temperature, viscosity contrast between pv and pPv, and the Clapeyron slope of pPv phase change. We observe that under certain conditions, pPv patches may be maintained at the edge and within reservoirs of dense, primordial material.

2. Model Setup

To perform our numerical experiments, we use the code StagYY [*Tackley*, 2008], which solves the conservation equations of mass, momentum, energy, and composition for an anelastic compressible fluid with infinite Prandtl number. All calculations are performed in 2-D spherical annulus geometry. The grid has radial and lateral resolutions of 256 and 512 cells, respectively, and is refined in the top and bottom 150 km, with best refined steps of 2 km. The composition field is tracked by about 2 million tracers and varies between 0 for regular mantle material and 1 for primordial dense material.

The viscosity is assumed to depend on temperature, depth, phase, and yield stress, and we further imposed a viscosity jump of 30 between upper and lower mantles. The viscosity is therefore given by

$$\eta = \frac{1}{\left(\frac{1}{\eta_b(z, T, \Gamma_{pPv})} + \frac{1}{\eta_Y} \right)}$$

with

$$\eta_b(z, T, \Gamma_{pPv}) = \eta_0 [1 + 29H(z - 660)] \exp \left[\Gamma_{pPv} ln(\Delta \eta_{pPv}) + V_a \frac{z}{D} + E_a \frac{\Delta T_S}{(T + T_{off})} \right]$$

and

$$\eta_Y = \frac{\sigma_0 + \sigma_i P}{2\dot{e}} \tag{1}$$

where η_0 is the reference viscosity (taken at temperature T=1600 K and depth $z = 0$ km), H the Heaviside step function, and $\Delta \eta_{pPv}$ the viscosity jump between perovskite and post-perovskite. V_a and E_a are the nondimensional activation volume and activation energy, controlling viscosity variations with depth and temperature, respectively, and T_{off} is the offset temperature, which reduces the viscosity jump through the top thermal boundary layer. In all our calculations, the value of this parameter is set to $0.88\Delta T_S$. The yield stress helps to build plate-like behavior at the top of the domain. Here we defined the yield stress by imposing its surface value σ_0 and its pressure gradient σ_i. The yield viscosity, η_Y, is defined as the ratio between the yield stress and the second invariant of the strain rate tensor $\dot{e}$. To avoid numerical difficulties, the viscosity is truncated between 10^{-3} and 10^5 of the reference viscosity.

The phase boundary from perovskite to post-perovskite is fixed at a reference point of 2700 K and 2700 km depth [e.g., *Murakami et al.*, 2004], from where lateral deviations in the depth are determined by using the phase function approach of *Christensen and Yuen* [1985] defined by

$$\Gamma_{pPv}(T, z) = 0.5 + 0.5 tanh \frac{z - z_{pPv} - \gamma_{pPv}(T - T_{pPv})}{w} \tag{2}$$

Table 1. Parameters of the Numerical Models

Parameter	Symbol	Value
Acceleration of gravity	g	9.81 m s^{-2}
Mantle thickness	D	2891 km
Superadiabatic temperature difference	ΔT_S	2500 K
Reference adiabatic temperature	T_{as}	1600 K
Surface density	ρ_S	3300 kg/m^3
CMB density	ρ_b	5500 kg/m^3
Surface thermal expansion	α_S	$5.0 \times 10^{-5} \text{ K}^{-1}$
CMB thermal expansion	α_b	$1.0 \times 10^{-5} \text{ K}^{-1}$
Surface thermal diffusivity	κ_S	$6.24 \times 10^{-7} \text{ m}^2\text{s}^{-1}$
CMB thermal diffusivity	κ_b	$8.74 \times 10^{-7} \text{ m}^2\text{s}^{-1}$
Clapeyron slope at $z = 660$ km	Γ_{660}	-2.5 MPa/K
Reference thermal viscosity	η_0	1.6×10^{21} Pa s
Viscosity ratio at $z = 660$ km	η_{660}	30
Thermal viscosity ratio	$\Delta\eta_T$	10^9
Vertical viscosity ratio	$\Delta\eta_Z$	10^2
Width of pv to pPv phase transition	w	10 km

where Γ_{pPv} is the phase function for post-perovskite, varying from 0 for perovskite to 1 for post-perovskite, T and z temperature and depth, respectively, (T_{pPv}, z_{pPv}) a point on the phase boundary, γ_{pPv} the Clapeyron slope, and w the width of the phase transition.

The reference Rayleigh number is defined as

$$Ra_{\text{ref}} = \frac{\alpha_s g \rho_s \Delta T_s D^3}{\eta_0 \kappa_s} \tag{3}$$

where α_s is the surface thermal expansivity, g the acceleration of gravity, ΔT_s the superadiabatic temperature difference, D the mantle thickness, η_0 the reference viscosity obtained using the potential temperature at the surface (here 1600 K), and κ_s the surface thermal diffusivity. This reference Rayleigh number is fixed at 10^8 in all experiments.

The primordial material is set to be denser than the regular mantle material, and the density contrast between primordial and regular mantle material is controlled by buoyancy ratio (B), which is defined as

$$B = \frac{\Delta\rho_C}{\alpha_s \rho_s \Delta T_s} \tag{4}$$

where $\Delta\rho_C$ is the density difference between the dense and regular material. The buoyancy ratio is fixed at 0.32 in all our experiments, which allows large primordial reservoirs to be stable at the bottom of the system [e.g., *Li et al.*, 2014a]. For a superadiabatic temperature difference $\Delta T_S = 2500$ K and thermal expansion $\alpha_s = 5.0 \times 10^{-5}$ (taken at $z = 0$ and $T = 1600$ K), this value of B leads to a density contrast of 130 kg/m^3, corresponding to a relative density anomaly of about 2.4% at the bottom of the mantle. This value is in agreement with estimates of density anomalies in the lowermost mantle from probabilistic tomography [e.g., *Trampert et al.*, 2004; *Mosca et al.*, 2012]. The initial thickness of the primordial layer is 0.07, i.e., 5% in total mantle volume. The values of other physical parameters are listed in Table 1.

3. Results

3.1. Influence of pPv Phase Transition Properties

We first conducted a series of experiments in which we vary the CMB temperature, T_{CMB}. We considered three values of T_{CMB}, 3350 K, 3475 K, and 3750 K, covering the range of values suggested by *Nomura et al.* [2014]. In this series of experiments, the viscosity of pPv is smaller than that of perovskite by 3 orders of magnitude (weak pPv) [*Ammann et al.*, 2010], and we set the Clapeyron slope to 13 MPa/K. We observe three main distribution patterns of pPv depending on T_{CMB}. For $T_{CMB} = 3350$ K, the outer core is fully covered by a layer of pPv, including within the reservoir of dense material (Figures 1a–1c). The thickness of the pPv layer varies with local pressure-temperature (P-T) conditions, with the pPv layer being thinner within the large primordial
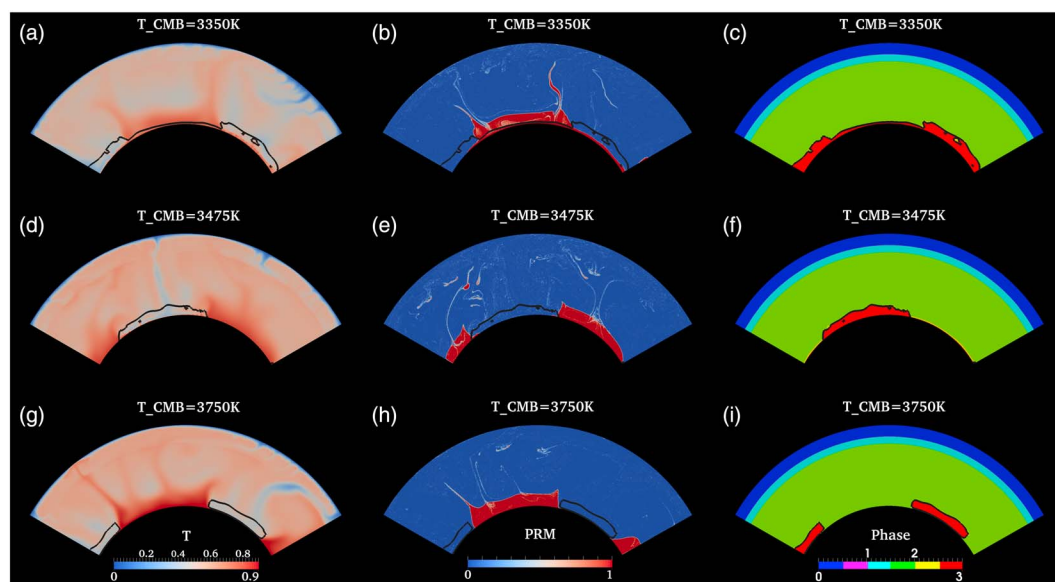
Figure 1. Snapshots of superadiabatic (a, d, and g) temperature, (b, e, and h) composition, and (c, f, and i) phase fields for experiments with different CMB temperature at $t = 5$ Gyr. The viscosity contrast between pPv and pv is 1/1000 in all three experiments. For the phase field, the colour code ranges from 0 to 3 for olivine, spinel, perovskite, and post-perovskite, respectively. The boundary of pv and pPv is contoured in black. Note that the magenta and yellow regions denote regions where two phases are present, due to the fact that in our model phase change is not discontinuous, but varies smoothly with temperature and pressure.

reservoirs, which are hotter than surrounding mantle material, and thicker in the regions where cold slab reaches the lowermost mantle. In contrast, for T_{CMB}=3750 K, we observe double crossing of the pPv phase change at the edge of the pPv piles and a strong anticorrelation between the location of pPv and that of large primordial reservoirs. For an intermediate CMB temperature, $T_{CMB} = 3475$ K, the primordial reservoirs are periodically pushed aside as cold downwellings reach the CMB, leading to the formation of a horizontal thin, long tail of primordial material at the margins of these reservoirs. The local P-T conditions at these margins are such that the phase change from pv to pPv can occur temporarily, i.e., the thin horizontal tail of primordial material is within the stability field of pPv. The thickness of the margins is typically of several tens of kilometers, and their length varies with time up to several hundred kilometers.

We then conducted a series of experiments to investigate the effects of the pPv viscosity, with the CMB temperature and pPv Clapeyron slope kept fixed and equal to 3475K and 13 MPa/K, respectively. It has been suggested that pPv may be less viscous than perovskite by at least 3 orders of magnitude [*Ammann et al.*, 2010], with possible implications for the mantle dynamics [*Nakagawa and Tackley*, 2011; *Samuel and Tosi*, 2012; *Li et al.*, 2014b]. We considered two cases: regular pPv ($\Delta\eta_{pPv} = 1$) and weak pPv ($\Delta\eta_{pPv}$=1/1000). In both cases, radial 1-D profiles of primordial dense material (Figure 2g) clearly show that most of the material is maintained in the lower mantle. However, primordial reservoirs in the experiment with weak pPv are overall less stable than those in the experiment with regular pPv. Comparison between Figures 2a–2c and Figures 2d–2f shows that there is more primordial material in the middle and upper mantle (above 2000 km) and slightly less primordial material in the lower mantle in the experiment with weak pPv than in the experiment with regular pPv. Figure 2g further indicates that in the depth range 700–1500 km the volume fraction of dense material remains around 3% for the weak pPv case and only 1% in the regular pPv case. A notable exception is the lowermost several tens of kilometers, where a thin long pPv primordial layer spread along the CMB. Again, in the experiment with weak pPv, sharp horizontal tails of dense material, in which pPv is stable, form at the margin of primordial reservoir, as cold slabs reach the deep mantle and push the primordial material aside (Figure 2e). Due to the viscosity contrast between pv and pPv, the low viscosity part in the deepest mantle is in the cold region where the pPv phase change occurs (Figure 2f), in agreement with previous studies [*Nakagawa and Tackley*, 2011; *Samuel and Tosi*, 2012; *Li et al.*, 2014b]. In the experiment with regular pPv, on the contrary, we do not observe horizontal tails (Figure 2b), and the pPv stability field is strongly anticorrelated with the primordial reservoirs.
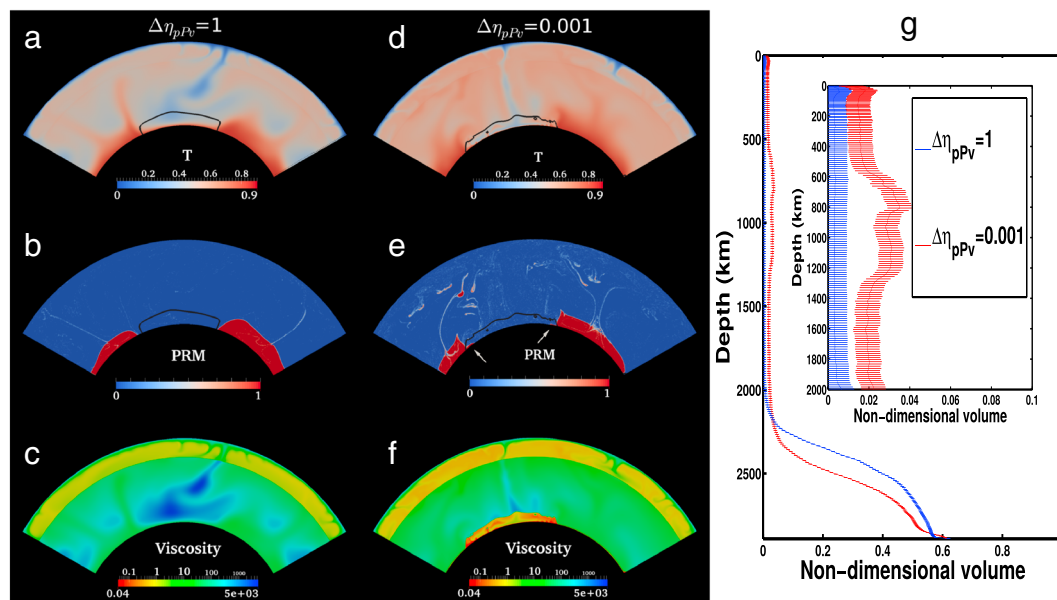
Figure 2. (a–f) Snapshots of superadiabatic temperature (Figures 2a and 2b), composition (Figures 2c and 2d), and viscosity (Figures 2e and 2f) fields for experiments with regular pPv ($\Delta\eta_{pPv} = 1$, Figures 2a, 2c, and 2e) and weak pPv ($\Delta\eta_{pPv} = 0.001$, Figures 2b, 2d, and 2f) at $t = 5$ Gyr. The CMB temperature is fixed at 3475 K. The boundary of pv and pPv is contoured in black. (g) One-dimensional profile of the average volume percentage of primordial material as a function of depth for these two experiments in the last 2 Gyr.

The Clapeyron slope is another important parameter that affects the presence of the pPv phase transition. Small Clapeyron slopes favor the occurrence of pPv, while large values prevent the presence of pPv above the CMB. The value of the Clapeyron slope may, in particular, control the presence of pPv patches within reservoirs of primordial material. The Clapeyron slope of the pPv phase transition is still uncertain, with early estimates in the range 4–8 MPa/K [*Oganov and Ono*, 2004] but more recent studies pointing to larger values of around 13 MPa/K and up to 17 MPa/K [e.g., *Tateno et al.*, 2009; *Dobson et al.*, 2011]. Previous calculations with setup similar to that of our experiments [*Li et al.*, 2015] have shown that values of the Clapeyron slope smaller than 10 MPa/K lead to pPv layering around the CMB, provided that the CMB temperature is not too high. Discontinuous pPv patches appear only for higher values of the Clapeyron slope, around 12 MPa/K and more. Here we only focus on this higher end of the range of Clapeyron slope. Figure 3 shows snapshots of experiments with low CMB temperature (3350 K), weak pPv, and different Clapeyron slopes at $t = 5$ Gyr. Figures 3a–3c show the experiment with a Clapeyron slope of 13 MPa/K. In this case, a pPv layer of different thickness covers the whole CMB region. This layer is thicker in cold regions, where cold slabs spread along the CMB, and thinner in hot regions such as the interior of large primordial reservoirs. As the Clapeyron slope increases to 15 MPa/K, the whole CMB region is still covered by a pPv layer, but the thickness of this layer strongly varies. In particular, it is very thin within the large primordial reservoirs (Figures 3d–3f). With an extreme value of 17 MPa/K, the phase change from pv to pPv hardly occurs within the large primordial reservoirs and even outside (Figures 3g–3i). Still in this case, we observe a strong anticorrelation between the locations of the pPv phase and large primordial reservoirs. "Double crossings" of the pPv phase change [*Hernlund et al.*, 2005] are also present.

3.2. Temporary pPv Patches Within Primordial Reservoirs

The three experiments shown in Figure 3 illustrate two main types of interface between pPv stability regions and large primordial reservoirs, namely, pPv fully covering the CMB and strong anticorrelation between pPv regions and primordial reservoirs. It further shows that pPv phase change may occur locally and temporarily within large primordial reservoirs, generating small discontinuous pPv patches. Figure 4 shows a sequence of snapshots of the thermal and compositional field for a similar experiment, in which small discontinuous pPv patches are generated. The CMB temperature is 3350 K, as in the experiments shown in Figure 3, the viscosity of pPv is 1/1000 that of perovskite (weak pPv), and the Clapeyron slope is 15.5 MPa/K, which is intermediate between the values leading to a full pPv layer and a strong anticorrelation between pPv and large primordial reservoirs. In Figures 4a and 4b, showing the temperature and compositional fields at $t = 3.753$ Gyr, small pPv
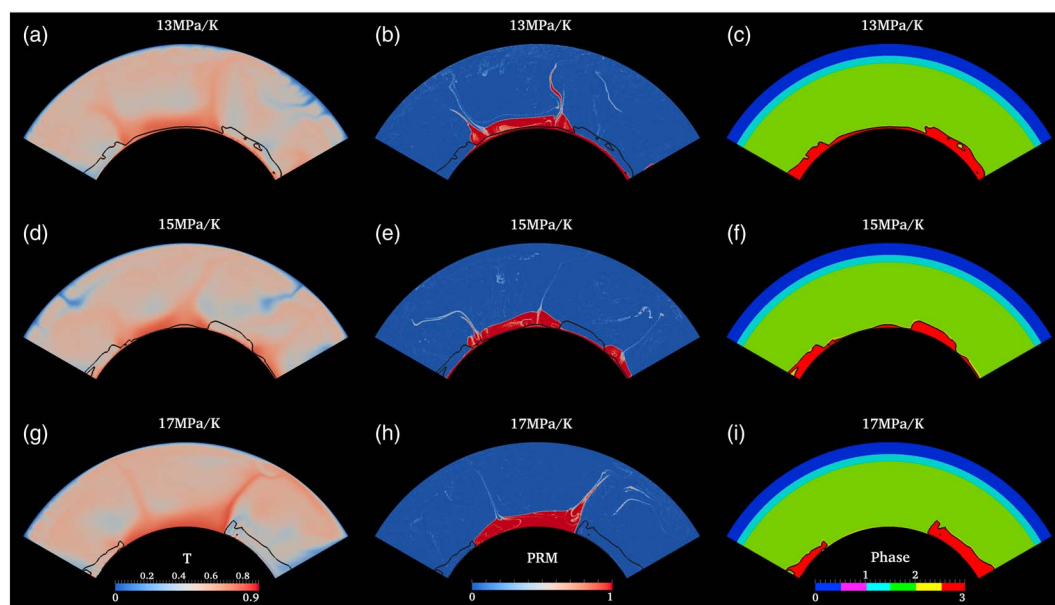
Figure 3. Snapshots of superadiabatic (a, d, and g) temperature, (b, e, and h) composition, and (c, f, and i) phase fields for experiments with low CMB temperature (T_{CMB} = 3350 K), weak pPv ($\Delta\eta_{pPv}$ = 0.001), and different Clapeyron slope (γ_{pPv} = 13, 15, and 17 MPa/K) at t = 5 Gyr. For the phase field, the colour code ranges from 0 to 3 for olivine, spinel, perovskite, and post-perovskite, respectively. The boundary of pv and pPv is contoured in black.

piles clearly appear at the base of large primordial reservoirs (see zoom in Figures 4j and 4t). We more precisely observe two types of pPv patches: small lenses located well within the reservoirs of primordial material and elongated patches at the thinned edges of the reservoirs, similar to those observed in our other experiments with weak pPv and an intermediate CMB temperature (Figures 1d–1f). As they reach the CMB, cold slabs push the large reservoirs aside, creating thin horizontal tails of primordial material. Due to interaction with cold slab, the tails of primordial materials become colder, allowing the pPv phase change to occur. These elongated pPv patches are typically a few tens of kilometers in height. Due to the downwellings waxing and waning, their length strongly varies with time, typically reaching a few hundreds of kilometers at a maximum. Importantly, while their size strongly varies with time, these tails are maintained for a long period of time even comparable to that of the large primordial reservoirs. In contrast, the pPv patches observed inside large primordial reservoirs are short-lived. The pPv patches are approximately 70 km in height and 350 km in length at a maximum in the primordial reservoir on the left half of the box (which is ∼2000 km long) and 20 km in height and 170 km in length in the primordial reservoir on the right half (which is ∼3000 km long)(Figure 4b). Figures 4c–4g show the time evolution of temperature and composition fields of the area in the left white box in Figure 4b. At the beginning of this sequence (t = 3.645 Gyr), the pPv phase is found only at the margin of large primordial reservoirs in the reservoir's thin horizontal tail. Then, starting at about t = 3.681 Gyr, the isotherms within the reservoir are locally depressed toward the CMB, due to the entrainment of regular, colder material within the dense reservoirs. This local decrease in temperature allows the phase change from pv to pPv to occur at the base of the primordial reservoir, leading to the formation of a pPv patch. This patch grows, reaches its largest size at about t = 3.753 Gyr and starts decreasing again after that time. At t = 3.942 Gyr and later times, the local P-T condition does not allow for maintaining pPv patches. In contrast, in the thin elongated edge of the reservoir, pPv can be maintained during the entire sequence. In this region, temperature varies less and remains low enough to allow the presence of pPv during the entire sequence. In addition, because the thickness of dense primordial material is much reduced in this region, the dynamic pressure is slightly smaller than in the reservoir interior, which contributes to the stability of pPv at this location. A similar evolution is observed in the primordial reservoir on the right half of the box (Figures 4m–4q), except that the pPv patch located in the interior of this reservoir is smaller and remains stable during a shorter period of time. Again, a thin tail of primordial material, in which pPv is stable, extends laterally at the margin of the reservoir.

To summarize, our experiment shows that if the CMB temperature is low enough, pPv patches can be temporarily maintained within the reservoirs of dense, primitive material, and at its edges. The small pPv patches
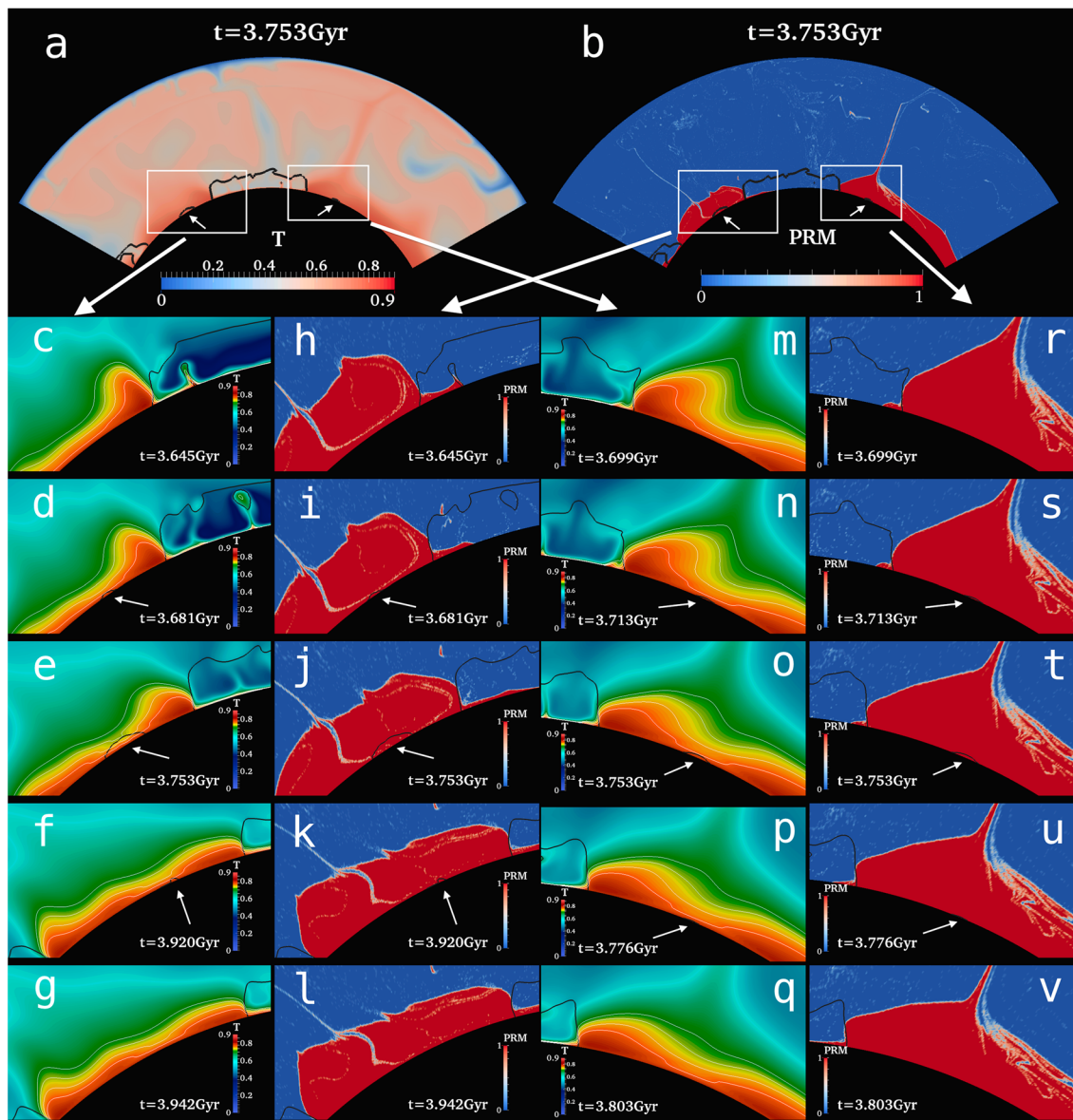
Figure 4. Snapshots of evolution of small discontinuous pPv piles within the large primordial reservoirs in the experiment with $T_{CMB} = 3350$ K and $\Gamma_{pPv} = 15.5$ MPa/K. The boundary of pv and pPv is contoured in black. Isosurfaces of superadiabatic temperature of 0.70, 0.72, 0.74, and 0.76 are contoured in white from top to bottom. All small pPv piles at the base of interior of large primordial reservoirs are indicated by small arrows. (a) Superadiabatic temperature field at $t = 3.753$ Gyr; (b) composition field at $t = 3.753$ Gyr. Evolution of (c–g) temperature and (h–l) composition fields of the left reservoir. Evolution of (m–q) temperature and (r–v) composition fields of the right reservoir.

in the interior of large primordial reservoirs are related to variations in the local P-T conditions at short time scale and are thus maintained for short periods of time, typically ~100 s Myr, whereas the pPv patches at the edge of the reservoirs are stable for longer period of time due to the fact that these regions are colder than the reservoirs' interiors.

4. Discussion and Conclusions

In this study, we investigate the distribution of the pPv phase relative to that of large reservoirs of primordial dense material as a function of the properties of the pPv phase change. We observe three cases within the possible value range of these properties: (1) for low values of the CMB temperature and of the Clapeyron slope, a full pPv layer covers the Earth's core, with lateral variations in thickness due to the local temperature and pressure conditions; (2) for large CMB temperature and Clapeyron slope, the stability region of pPv is

strongly anticorrelated with the location of large primordial reservoirs; and (3) for low CMB temperature and Clapeyron slope around 15.5 MPa/K, small pPv patches are temporarily stable within the primordial reservoirs and at their margins. In this later case, two sorts of pPv patches are generated: patches at the thin, elongated margins of the reservoirs, in which pPv is stable for relatively long periods of time (comparable to that of primordial reservoirs themselves) and internal patches, which are short-lived (~100 s Myr). Weak pPv, defined as pPv with a viscosity smaller than that of perovskite by 3 orders of magnitude, facilitates the phase change at the margins of large primordial reservoirs, while increasing Clapeyron slope plays an opposite role.

In our experiments, we focus on moderate to low (<3750 K) CMB temperature and high (>10 MPa/K) Clapeyron slope of pPv, which favors the generation of discontinuous pPv patches. Previous calculations [*Li et al.*, 2015] indicate that for higher CMB temperatures (around 4200 K and higher) pPv is unstable throughout the primordial reservoirs and that low (<10 MPa/K) Clapeyron slope lead to smoother variations of the pPv stability field, including full pPv layering around the CMB. Our conclusions are therefore not valid for high CMB temperatures and/or small values of the Clapeyron slope. It is important to note, however, that models of mantle dynamics that best explain available geophysical observations, including constraints on the D″ layer, tomographic models, and plume distribution, should include a moderate CMB temperature (around 3750 K) and a large Clapeyron slope (>13 MPa/K) [*Li et al.*, 2015].

In our experiments, small pPv patches within large primordial reservoirs appear preferentially at the margins of these reservoirs rather than in their interiors. In most of our experiments, weak pPv favors the formation at the margin of reservoirs of thin horizontal tails of primordial material, where pPv is stable. The detailed size and shape of these structures are affected by the cold slab and are therefore time dependent. Their height typically varies from a few tens of kilometers up to 100 km, and their length is up to several hundreds of kilometers. The presence of pPv patches within the interiors of large primordial reservoirs requires more specific and restricted ranges of pPv properties. For example, in experiments with low CMB temperature (3350 K), a Clapeyron slope smaller than 15 MPa/K leads to a full pPv layer above the CMB (Figures 3c and 3f), while a Clapeyron slope of 17 MPa/K leads to pPv phase change occurring only outside large primordial reservoirs. Only in a narrow range of the values of the Clapeyron slope may pPv occur locally within the large primordial reservoirs, as shown in Figure 4.

Our results have some interesting implications for the ultralow-velocity zones (ULVZs), supporting the hypothesis that these zones consist of iron pPv lenses. Shear wave velocity propagates faster in magnesium pPv than in perovskite. Therefore, if Mg-pPv patches are present within LLSVPs, they should locally induce fast shear wave velocity anomalies compared to the rest of the LLSVPs. No such observation has been reported so far, suggesting that if present, pPv patches within LLSVPs should be strongly enriched in iron, in which case they would be slower than average and may explain ULVZs. The large low shear wave velocity provinces (LLSVPs) may be explained by an enrichment in iron compared to surrounding mantle [e.g., *Trampert et al.*, 2004; *Mosca et al.*, 2012]. Following this hypothesis, post-perovskite patches forming within the LLSVPs would be also enriched in iron. Furthermore, iron-rich pPv transforms at lower pressure than pure magnesium pPv and, at a given pressure, remains stable up to higher temperature [e.g., *Stackhouse and Brodholt*, 2008]. This implies that pPv patches may be present within LLSVPs even for CMB temperatures higher than those we considered in our experiments and that these patches would be strongly enriched in iron. Based on mineral physics experiments, *Mao et al.* [2006] showed that the post-perovskite silicate phase containing up to 40% $FeSiO_3$ can result in reductions of *P* and *S* wave velocities of up to 13% and 44% at 130 GPa and 3000 K, somewhat larger than the decrease observed in ULVZs. These experiments further indicated that an iron content lower than 40% or an additional solid phase such as magnesiwüstite would bring the values into agreement with those observed in ULVZs [*Lay et al.*, 1998; *Wen and Helmberger*, 1998; *Thorne and Garnero*, 2004]. In addition, recent measurements [*Dorfman and Duffy*, 2014] suggested that the increase in density in ULVZs may be explained by a local iron enrichment about 40% in pPv. Therefore, pPv lenses within iron-rich reservoirs, e.g., LLSVPs, may have a seismic signature comparable to that of ULVZs. It should further be noted that our experiments exclude the possibility that ULVZs are related to the presence of partial melt, since the CMB temperatures we used [*Nomura et al.*, 2014] are much lower than those required to maintain partial melt [*Williams and Garnero*, 1996; *Berryman*, 2000].

Further comparisons between our results and observations of ULVZs [*Garnero*, 2000; *Thorne and Garnero*, 2004; *McNamara et al.*, 2010] can be made. First, the height of pPv patches at margins and interiors of large primordial reservoirs are comparable to the observed thickness of ULVZs. The height of pPv patches within

the large primordial reservoirs observed in our models are typically up to several tens of kilometers and down to below our highest resolution (<2 km). The patches at the margins of the reservoirs are slightly thinner than the internal patches, but their thickness is still around a few tens of kilometers. Second, while their size is time dependent, the pPv patches do not exceed a few hundreds of kilometers in length. Again, this fits well the observed lengths of ULVZs. It is also interesting to point out that internal pPv patches are usually smaller than those at the margins. Finally, in our experiments, pPv patches are present both at the margins and within interiors of large primordial reservoirs. This is consistent with the observed distribution of ULVZs, showing that most of the ULVZs are located within or at the margins of LLSVPs [*McNamara et al.*, 2010]. It is interesting to note that as shown in Figure 4, the locations of the small pPv piles within the interior of large primordial reservoirs are under or close to the roots of plumes above, which is again consistent with available observation of ULVZs [e.g., *Williams et al.*, 1998]. In addition, the extension of the thin elongated pPv primordial layers at the margins of primordial reservoirs are similar to the structures and size recently observed by high- resolution *P* wave tomography [e.g., *Frost and Rost*, 2014]. It should be noted, however, that ULVZs are also observed outside LLSVPs, which our experiments do not explain. ULVZs may thus have different origins depending on their location. Alternatively, small piles of primordial material, unresolved by current tomographic models, may exist locally in the lowermost mantle with P-T conditions allowing the presence of pPv. Such small piles are generated episodically in our models.

Another possible explanation for ULVZs is that they consist of lenses of dense, chemically distinct material within LLSVPs, which are themselves chemically distinct from the ambient mantle [e.g., *McNamara et al.*, 2010; *Thorne et al.*, 2013]. Like pPv patches, this hypothesis explains well the size and distribution of ULVZs, but it predicts a different time evolution of these structures, both in size and location. The numerical models of *McNamara et al.* [2010], which include large reservoirs of primordial material (modeling LLSVPs) and small patches of high-density material (modeling the ULVZs), indicate that the patches of high-density material are entrained by the internal flow of the primordial reservoir toward the margins of these reservoirs, where they tend to merge. In contrast, if ULVZs observed in LLSVPs are pPv patches enriched in iron, their locations should be relatively unchanged during their whole life time. Instead of moving to margins, the ULVZs located in the interiors of LLSVPs would appear or disappear depending on the P-T conditions in this region. The experiments of *McNamara et al.* [2010] further suggest that small amounts of high-density material may be entrained upward by thermal plumes generated at the edges of primordial reservoirs, thus inducing small changes in the size of ULVZs. The pPv patches hypothesis implies a more substantial time variation of the size of ULVZ. While the total volume of ULVZs may overall increase with time, due to core cooling, the size of the ULVZs may strongly vary with time at short (~100 Myr) time scales, following the evolution of local P-T conditions within the LLSVPs. At the current stage of our knowledge of the lower mantle, it is difficult to discriminate between the chemically distinct material and pPv patches hypotheses. This would require tracking the evolution of ULVZs over time scale of at least ~100 Myr. Seismic anisotropy in the lowermost mantle may provide additional information. In particular, strong anisotropy within or at the top of ULVZs may indicate that these regions experience strong shear stress, which might be related to strong horizontal flow due to their migration, thus supporting a chemically different origin for ULVZs [*McNamara et al.*, 2010]. Such observations are however currently not available.

Future works may focus on several directions. First, we treated the phase change from pv to pPv only as temperature and pressure dependent. However, as noted above, this phase change may also depend on composition, especially the iron component [e.g., *Stackhouse and Brodholt*, 2008]. The phase boundary may thus vary due to the composition, and a composition-dependent pPv phase change needs to be included into our model to fully investigate this effect. Second, because the pPv phase change is very sensitive to the change of P-T conditions in the lowermost mantle, accurate estimates of the size and duration of small pPv patches within the interior of large primordial reservoirs require an accurate description of mantle convection. Most of the parameters, including the density contrast between primordial and regular materials and the volume of LLSVPs, are poorly constrained. Previous studies [e.g., *Li et al.*, 2014a, 2015] have, however, identified ranges of likely values for these parameters (i.e., explaining several geophysical constraints observations), which we use in this study. While using these ranges of parameters, which ensures the presence of stable reservoirs of primordial material, it is important to check their influence on the distribution of pPv above the CMB. Third, high-resolution calculations in full 3-D spherical geometry are needed to investigate the detailed shape and distribution of these pPv patches at the margins and within the interiors of the large primordial reservoirs. These may further be used for quantitative comparisons with available seismological observations.

References

Ammann, M., J. Brodholt, J. Wookey, and D. Dobson (2010), First-principles constraints on diffusion in lower-mantle minerals and a weak D″ layer, *Nature*, *465*(7297), 462–465, doi:10.1038/nature09052.

Andrault, D., G. Pesce, M. A. Bouhifd, N. Bolfan-Casanova, J.-M. Hénot, and M. Mezouar (2014), Melting of subducted basalt at the core-mantle boundary, *Science*, *344*(6186), 892–895.

Berryman, J. G. (2000), Seismic velocity decrement ratios for regions of partial melt in the lower mantle, *Geophys. Res. Lett.*, *27*(3), 421–424, doi:10.1029/1999GL008402.

Christensen, U. R., and D. A. Yuen (1985), Layered convection induced by phase transitions, *J. Geophys. Res.*, *90*(B12), 10,291–10,300, doi:10.1029/JB090iB12p10291.

Davies, D. R., S. Goes, J. Davies, B. Schuberth, H.-P. Bunge, and J. Ritsema (2012), Reconciling dynamic and seismic models of Earth's lower mantle: The dominant role of thermal heterogeneity, *Earth Planet. Sci. Lett.*, *353–354*, 253–269, doi:10.1016/j.epsl.2012.08.016.

Dobson, D. P., S. A. Hunt, A. Lindsay-Scott, and I. G. Wood (2011), Towards better analogues for $MgSiO_3$ post-perovskite: $NaCoF_3$ and $NaNiF_3$, two new recoverable fluoride post-perovskites, *Phys. Earth Planet. Inter.*, *189*(3), 171–175.

Dorfman, S., and T. Duffy (2014), Effect of Fe-enrichment on seismic properties of perovskite and post-perovskite in the deep lower mantle, *Geophys. J. Int.*, *197*(2), 910–919, doi:10.1093/gji/ggu045.

Frost, D. A., and S. Rost (2014), The P-wave boundary of the large-low shear velocity province beneath the Pacific, *Earth Planet. Sci. Lett.*, *403*, 380–392, doi:10.1016/j.epsl.2014.06.046.

Garnero, E. J. (2000), Heterogeneity of the lowermost mantle, *Annu. Rev. Earth Planet. Sci.*, *28*(1), 509–537, doi:10.1146/annurev.earth.28.1.509.

He, Y., and L. Wen (2012), Geographic boundary of the Pacific anomaly and its geometry and transitional structure in the north, *J. Geophys. Res.*, *117*, B09308, doi:10.1029/2012JB009436.

Helmberger, D., S. Ni, L. Wen, and J. Ritsema (2000), Seismic evidence for ultralow-velocity zones beneath Africa and eastern Atlantic, *J. Geophys. Res.*, *105*(B10), 23,865–23,878.

Hernlund, J. W., C. Thomas, and P. J. Tackley (2005), A doubling of the post-perovskite phase boundary and structure of the Earth's lowermost mantle, *Nature*, *434*(7035), 882–886.

Ishii, M., and J. Tromp (1999), Normal-mode and free-air gravity constraints on lateral variations in velocity and density of Earth's mantle, *Science*, *285*(5431), 1231–1236, doi:10.1126/science.285.5431.1231.

Lay, T., and D. V. Helmberger (1983), A shear velocity discontinuity in the lower mantle, *Geophys. Res. Lett.*, *10*(1), 63–66, doi:10.1029/GL010i001p00063.

Lay, T., Q. Williams, and E. J. Garnero (1998), The core-mantle boundary layer and deep Earth dynamics, *Nature*, *392*(6675), 461–468.

Li, Y., F. Deschamps, and P. J. Tackley (2014a), The stability and structure of primordial reservoirs in the lower mantle: Insights from models of thermochemical convection in three-dimensional spherical geometry, *Geophys. J. Int.*, *199*(2), 914–930, doi:10.1093/gji/ggu295.

Li, Y., F. Deschamps, and P. J. Tackley (2014b), Effects of low-viscosity post-perovskite on the stability and structure of primordial reservoirs in the lower mantle, *Geophys. Res. Lett.*, *41*, 7089–7097, doi:10.1002/2014GL061362.

Li, Y., F. Deschamps, and P. J. Tackley (2015), Effects of the post-perovskite phase transition properties on the stability and structure of primordial reservoirs in the lower mantle of the Earth, *Earth Planet. Sci. Lett.*, *432*, 1–12, doi:10.1016/j.epsl.2015.09.040.

Mao, W. L., H.-k. Mao, W. Sturhahn, J. Zhao, V. B. Prakapenka, Y. Meng, J. Shu, Y. Fei, and R. J. Hemley (2006), Iron-rich post-perovskite and the origin of ultralow-velocity zones, *Science*, *312*(5773), 564–565.

Masters, G., G. Laske, H. Bolton, and A. Dziewonski (2000), The relative behavior of shear velocity, bulk sound speed, and compressional velocity in the mantle: Implications for chemical and thermal structure, in *Earth's Deep Interior: Mineral Physics and Tomography From the Atomic to the Global Scale*, edited by S. Karato et al., pp. 63–87, AGU, Washington, D. C.

McNamara, A. K., E. J. Garnero, and S. Rost (2010), Tracking deep mantle reservoirs with ultra-low velocity zones, *Earth Planet. Sci. Lett.*, *299*(1), 1–9.

Mosca, I., L. Cobden, A. Deuss, J. Ritsema, and J. Trampert (2012), Seismic and mineralogical structures of the lower mantle from probabilistic tomography, *J. Geophys. Res.*, *117*, B06304, doi:10.1029/2011JB008851.

Murakami, M., K. Hirose, K. Kawamura, N. Sata, and Y. Ohishi (2004), Post-perovskite phase transition in $MgSiO_3$, *Science*, *304*(5672), 855–858, doi:10.1126/science.1095932.

Nakagawa, T., and P. J. Tackley (2005), The interaction between the post-perovskite phase change and a thermo-chemical boundary layer near the core–mantle boundary, *Earth Planet. Sci. Lett.*, *238*(1), 204–216.

Nakagawa, T., and P. J. Tackley (2011), Effects of low-viscosity post-perovskite on thermo-chemical mantle convection in a 3-D spherical shell, *Geophys. Res. Lett.*, *38*, L04309, doi:10.1029/2010GL046494.

Ni, S., E. Tan, M. Gurnis, and D. Helmberger (2002), Sharp sides to the African superplume, *Science*, *296*(5574), 1850–1852, doi:10.1126/science.1070698.

Nomura, R., K. Hirose, K. Uesugi, Y. Ohishi, A. Tsuchiyama, A. Miyake, and Y. Ueno (2014), Low core-mantle boundary temperature inferred from the solidus of pyrolite, *Science*, *343*(6170), 522–525, doi:10.1126/science.1248186.

Oganov, A. R., and S. Ono (2004), Theoretical and experimental evidence for a post-perovskite phase of $MgSiO_3$ in Earth's D″ layer, *Nature*, *430*(6998), 445–448.

Rost, S., and J. Revenaugh (2003), Small-scale ultralow-velocity zone structure imaged by ScP, *J. Geophys. Res.*, *108*(B1), 2056, doi:10.1029/2001JB001627.

Rost, S., P. S. Earle, P. M. Shearer, D. A. Frost, and N. D. Selby (2015), Seismic detections of small-scale heterogeneities in the deep Earth, in *The Earth's Heterogeneous Mantle*, pp. 367–390, Springer, Switzerland.

Samuel, H., and N. Tosi (2012), The influence of post-perovskite strength on the Earth's mantle thermal and chemical evolution, *Earth Planet. Sci. Lett.*, *323-324*, 50–59, doi:10.1016/j.epsl.2012.01.024.

Sidorin, I., M. Gurnis, and D. V. Helmberger (1999), Dynamics of a phase change at the base of the mantle consistent with seismological observations, *J. Geophys. Res.*, *104*(B7), 15,005–15,023, doi:10.1029/1999JB900065.

Stackhouse, S., and J. P. Brodholt (2008), Elastic properties of the post-perovskite phase of Fe_2O_3 and implications for ultra-low velocity zones, *Phys. Earth Planet. Inter.*, *170*(3), 260–266.

Sun, D., D. V. Helmberger, J. M. Jackson, R. W. Clayton, and D. J. Bower (2013), Rolling hills on the core-mantle boundary, *Earth Planet. Sci. Lett.*, *361*(0), 333–342, doi:10.1016/j.epsl.2012.10.027.

Tackley, P. J. (2008), Modelling compressible mantle convection with large viscosity contrasts in a three-dimensional spherical shell using the Yin-Yang grid, *Phys. Earth Planet. Inter.*, *171*(1–4), 7–18, doi:10.1016/j.pepi.2008.08.005.

Tackley, P. J. (2012), Dynamics and evolution of the deep mantle resulting from thermal, chemical, phase and melting effects, *Earth Sci. Rev.*, *110*(1–4), 1–25, doi:10.1016/j.earscirev.2011.10.001.

Tateno, S., K. Hirose, N. Sata, and Y. Ohishi (2009), Determination of post-perovskite phase transition boundary up to 4400 K and implications for thermal structure in D″ layer, *Earth Planet. Sci. Lett.*, *277*(1–2), 130–136, doi:10.1016/j.epsl.2008.10.004.

Thorne, M. S., and E. J. Garnero (2004), Inferences on ultralow-velocity zone structure from a global analysis of SPdKS waves, *J. Geophys. Res.*, *109*, B08301, doi:10.1029/2004JB003010.

Thorne, M. S., E. J. Garnero, G. Jahnke, H. Igel, and A. K. McNamara (2013), Mega ultra low velocity zone and mantle flow, *Earth Planet. Sci. Lett.*, *364*, 59–67.

Trampert, J., F. Deschamps, J. Resovsky, and D. Yuen (2004), Probabilistic tomography maps chemical heterogeneities throughout the lower mantle, *Science*, *306*(5697), 853–856, doi:10.1126/science.1101996.

Tsuchiya, T., J. Tsuchiya, K. Umemoto, and R. M. Wentzcovitch (2004), Phase transition in $MgSiO_3$ perovskite in the Earth's lower mantle, *Earth Planet. Sci. Lett.*, *224*(3–4), 241–248, doi:10.1016/j.epsl.2004.05.017.

van der Hilst, R. D., and H. Kárason (1999), Compositional heterogeneity in the bottom 1000 kilometers of Earth's mantle: Toward a hybrid convection model, *Science*, *283*(5409), 1885–1888.

Wang, Y., and L. Wen (2007), Geometry and P and S velocity structure of the African anomaly, *J. Geophys. Res.*, *112*, B05313, doi:10.1029/2006JB004483.

Wen, L., and D. V. Helmberger (1998), Ultra-low velocity zones near the core-mantle boundary from broadband PKP precursors, *Science*, *279*(5357), 1701–1703.

Williams, Q., and E. J. Garnero (1996), Seismic evidence for partial melt at the base of Earth's mantle, *Science*, *273*(5281), 1528–1530.

Williams, Q., J. Revenaugh, and E. Garnero (1998), A correlation between ultra-low basal velocities in the mantle and hot spots, *Science*, *281*(5376), 546–549.